U–Pb zircon, geochemical and Sr–Nd–Hf isotopic constraints on age and origin of Jurassic I- and A-type granites from central Guangdong, SE China: A major igneous event in response to foundering of a subducted flat-slab?

Xian-Hua Li [a,b,*], Zheng-Xiang Li [c], Wu-Xian Li [a], Ying Liu [a], Chao Yuan [a], Gangjian Wei [a], Changshi Qi [a]

[a] *Key Laboratory of Isotope Geochronology and Geochemistry, Guangzhou Institute of Geochemistry, Chinese Academy of Sciences, Guangzhou 510640, China*
[b] *State Key Laboratory of Lithospheric Evolution, Institute of Geology and Geophysics, Chinese Academy of Sciences, Beijing 100029, China*
[c] *Tectonics Special Research Centre, School of Earth and Geographical Sciences, The University of Western Australia, Crawley, WA 6009, Australia*

Abstract

The Mesozoic geology of SE China is characterized by widespread Jurassic to Cretaceous igneous rocks consisting predominantly of granites and rhyolites and subordinate mafic lithologies. However, the tectonic regime responsible for the inland Jurassic granites remains controversial. We report here U–Pb zircon ages, geochemical and Sr–Nd–Hf isotopic data for the Nankunshan alkaline granite and the Fogang granitic batholith in central Guangdong. Mineralogical and geochemical features suggest that the Fogang and Nankunshan rocks are I- and aluminous A-type granites, respectively. SHRIMP U–Pb zircon analyses yield consistent ages ranging from 159 ± 3 Ma to 165 ± 2 Ma for four samples from the Fogang Batholith, and an age of 158 ± 5 Ma for the Nankunshan Granite. The Fogang granites, having $I_{Sr} = 0.7098 – 0.7136$, $\varepsilon Nd(T) = -4.3$ to -12.2 and $\varepsilon Hf(T) = -11.5$ to -3.1 for the magmatic zircons, were derived from Paleoproterozoic mafic-intermediate igneous protolith with minor addition of mantle-derived magmas. The Nankunshan rocks have relatively lower $I_{Sr} \approx 0.706 – 0.708$, higher $\varepsilon Nd(T) = 0.3$ to -2.4 and $\varepsilon Hf(T) = -5.7$ to 1.1 for the magmatic zircons, and some OIB-like trace element ratios. They were likely generated through extensive fractional crystallization of mantle-derived alkaline parental magma associated with crustal assimilation. These ~ 160 Ma I- and A-type granites in central Guangdong were emplaced coeval with the widespread 165–155 Ma I- and A-type granites and syenites following the initiation of intraplate basaltic and/or bimodal igneous magmatism at 180–170 Ma in the adjacent regions. We interpret these Jurassic igneous rocks as anorogenic magmatism formed during a major igneous event in response to foundering of an early Mesozoic subducted flat-slab beneath SE China continent.
© 2006 Elsevier B.V. All rights reserved.

Keywords: Granites; U–Pb zircon age; Geochemistry; Sr–Nd–Hf isotopes; Jurassic; Lithosphere foundering; SE China

* Corresponding author. Key Laboratory of Isotope Geochronology and Geochemistry, Guangzhou Institute of Geochemistry, Chinese Academy of Sciences, Guangzhou 510640, China. Fax: +86 20 85291510.
E-mail address: lixh@gig.ac.cn (X.-H. Li).

1. Introduction

The Mesozoic geology of Southeastern (SE) China is characterized by widespread igneous rocks consisting predominantly of granites and rhyolites and subordinate mafic intrusive and volcanic rocks. In addition to the sporadically-distributed Triassic (referred to as "Indosinian" in Chinese literature) intrusions (Wang et al., 2005a), the late Mesozoic ("Yanshanian") igneous rocks fall into two main age groups, i.e. the Jurassic ("Early Yanshanian") and the Cretaceous ("Late Yanshanian") (e.g. Li, 2000; Zhou and Li, 2000). There seems to be an ocean-ward younging trend for these Yanshanian igneous rocks, with the Jurassic rocks in the inland, and the Cretaceous rocks along the coastal areas (Fig. 1a), despite precise timing of many rocks still awaits further high-precision geochronology investigations.

The Yanshanian granites and associated numerous non-ferrous and rare metal mineral deposits in SE China have attracted much attention from the international geoscience community since 1940s. However, the tectonic regime responsible for the Yanshanian magmatism is still a matter of debate. Different models have been proposed in the last two decades. Amongst them, the active continental margin model related to the subduction of the paleo-Pacific plate beneath the Eurasia plate has been prevalent (e.g. Jahn et al., 1976; Holloway, 1982; Charvet et al., 1994; Martin et al., 1994; Lan et al., 1996; Lapierre et al., 1997; Sewell and Campbell, 1997). This model, however, does not explain why the magmatic belt is >1000-km-wide. Recently, Zhou and Li (2000) proposed a change in the slab dip angle of the subducting paleo-Pacific plate beneath SE China from a very low angle in early Jurassic to a medium angle in late Cretaceous, which they use to accommodate the exceptionally-wide magmatic province. This modified subduction model still fails to explain the intraplate nature of the Jurassic magmatism.

An alternative intraplate extension and/or rifting regime (Gilder et al., 1991; Li, 2000) has been proposed to account for the development of subordinate rifting-related alkaline basalts and syenites (Li et al., 2004a; Wang et al., 2004), bimodal volcanic and intrusive rocks (Chen et al., 1999; Li et al., 2003a; Wang et al., 2005c) and mafic dykes in SE China hinterland (Li and McCulloch, 1998). However, it was unclear what tectonic process drove the intraplate extension. Li and Li (2007) recently proposed a flat-slab subduction and slab-foundering model to account for both the wide Indosinian orogen and the broad Mesozoic magmatic province.

In order to verify the various models, systematic geochronological, geochemical and isotopic investiga-tions of all the Mesozoic igneous rocks are needed. In this paper we present SHRIMP U–Pb ages, major and trace element geochemistry and Sr–Nd–Hf isotope data for the Jurassic granites in the central Guangdong Province, and use these data to discuss the petrogenesis and tectonic implications.

2. Geological background

The Early Yanshanian (ca. 190–150 Ma) granitoids in SE China hinterland are mainly distributed north-easterly along the Wuyishan Mountains and adjacent regions to the east, and along the EW-trending Nanling Ranges to the southwest (Fig. 1a). The total exposed area of these granitoids is estimated at ca. 75,000 km^2.

The Fogang Batholith outcrops along the southern slope of the Nanling Ranges in central Guangdong Provinces with a total exposed area of ~6000 km^2, including the main body of Fogang Granite, the easterly elongated Xinfengjiang Pluton, and the Lapu Pluton to the southeast (Fig. 1b). Coarse-grained biotite monzo-granite and syenogranite with K-feldspar megacrysts are the dominant rock types, making up ca. 85% of the whole batholith. They contain 25–40% quartz, 25–45% K-feldspar, 20–45% plagioclase (An$_{15-35}$), 2–8% biotite, 0–5% hornblende, 0–1% muscovite and trace amounts of zircon, apatite, allanite, titanite, magnetite and ilmenite. Subordinate granodiorite, fine-grained biotite granite, two-mica granite and granite porphyry make up the remainder of the batholith. Mafic microgranular enclaves are common in the granodiorite and monzo-granite (Xu et al., 2002). The Fogang Batholith intruded the Late Neoproterozoic to Early Jurassic sedimentary rocks, and was in turn intruded by the Ejinao nepheline sodalite syenite dated at 137±2 Ma (Wang et al., 2005b). The granites are neither deformed nor metamorphosed.

The Fogang Batholith is a good lithological repre-sentative for the early Yanshanian granites in SE China. Although a number of studies were carried out on the mineralogy, petrology, geochemistry and isotopic age determinations (Zhuang et al., 2000; Chen et al., 2002; Xu et al., 2002; Bao and Zhao, 2003), the age and petrogenesis of the granites remain controversial. Even the genetic classification for the Fogang granites is debated, including the S-type (e.g. Guangdong, 1988; Chen et al., 2002), I-type (Zhuang et al., 2000) and aluminous A-type (Bao and Zhao, 2003).

The Nankunshan granite outcrops over ca. 200 km^2 to the southeast of the Fogang Batholith. It intruded the Middle Jurassic Gaojiping Formation volcanic rocks and monzogranite of the Fogang Batholith (Fig. 1b). The granites are commonly light grey to pink in color
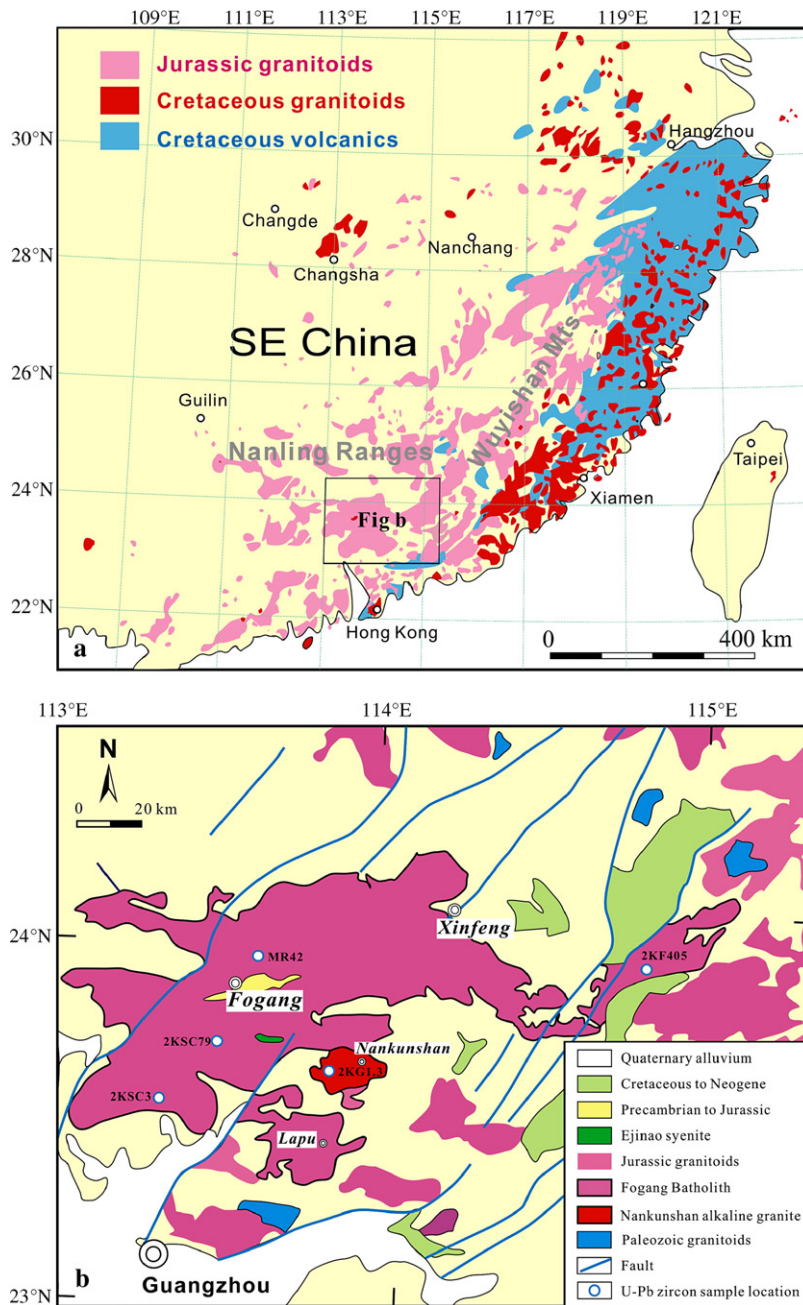
Fig. 1. (a) Distribution of the Yanshanian igneous rocks in southeastern China; (b) simplified geological map of central Guangdong Province (modified after Guangdong, 1988).

owing to the abundance of cream-white to brick-red colored K-feldspar crystals. They are composed of 23–36% quartz, 24–48% perthite, 14–18% albite plagioclase (An_{0-5}), 2–5% annite, 0.3–0.5% muscovite, and minor amount of fluorite, typical of alkaline granite (Liu et al., 2003). Accessory minerals include zircon, monazite, niobite, allanite and apatite. The Nankunshan granite is commonly considered as aluminous A-type

(Bao and Zhao, 2003; Liu et al., 2003), but its formation age is poorly constrained between 111 ± 16 Ma and 147 ± 0.8 Ma (Liu et al., 2003, 2005a).

3. Analytical procedures

Zircons were separated from five granite samples using standard density and magnetic separation techniques.

Representative zircon grains were hand-picked under a binocular microscope. Zircon grains, together with a zircon U–Pb standard TEMORA, were cast in an epoxy mount, which was then polished to section the crystals in half for analysis. Zircons were documented with transmitted and reflected light micrographs as well as cathodoluminescence (CL) images to reveal their internal structures, and the mount was vacuum-coated with a ca. 500-nm-thick layer of high-purity gold. Measurements of U, Th, and Pb were conducted using a SHRIMP II ion microprobe at the Beijing SHRIMP Center in the Institute of Geology, Chinese Academy of Geological Sciences. U–Th–Pb ratios were determined relative to the TEMORA standard zircon ($^{206}Pb/^{238}U$ = 0.0668 corresponding to 417 Ma, Black et al., 2003), and the absolute abundances were calibrated to the SL13 standard zircon (^{238}U = 238 ppm). Analyses of the TEMORA standard zircons were interspersed with those of unknown grains, following operating and data processing procedures similar to those described by Williams (1998). Measured compositions were corrected for common Pb using the ^{204}Pb-method. Uncertainties on individual analyses are reported at 1σ level; mean ages for pooled $^{206}Pb/^{238}U$ results are quoted at 95% confidence level. SHRIMP U–Pb zircon data for five granite samples are presented in Data Repository Table 1.

Major element oxides were determined by standard XRF on a Rigaku ZSX100e instrument. Analytical uncertainties range from 1% to 5%. Trace elements were analyzed using a Perkin-Elmer Sciex ELAN 6000 ICP-MS, and the analytical procedures are similar to those described by Li (1997a). About 50 mg of powdered sample was dissolved in high-pressure Teflon bombs using a HF+HNO$_3$ mixture. Rh was used as an internal standard to monitor signal drift during counting. The USGS rock standards GSP-1, G-2, W-2 and AGV-1 and the Chinese national rock standards GSR-1 and GSR-3 were chosen for calibrating element concentrations of measured samples. Analytical uncertainties were generally <5%. The data are listed in Data Repository Tables 2 and 3.

Sr and Nd isotopic analyses were performed on a Micromass Isoprobe multi-collector ICPMS, using analytical procedures described by Wei et al. (2002) and Li et al. (2004b). Sr and REE were separated using cation columns, and Nd fractions were further separated by HDEHP-coated Kef columns. Measured $^{87}Sr/^{86}Sr$ and $^{143}Nd/^{144}Nd$ ratios were normalized to $^{86}Sr/^{88}Sr$ = 0.1194 and $^{146}Nd/^{144}Nd$ = 0.7219, respectively. The reported $^{87}Sr/^{86}Sr$ and $^{143}Nd/^{144}Nd$ ratios were respectively adjusted to the NBS SRM 987 standard $^{87}Sr/^{86}Sr$ = 0.71025 and the Shin Etsu JNdi-1 standard $^{143}Nd/^{144}Nd$ = 0.512115. The results, along with the calculated initial

$^{87}Sr/^{86}Sr$ (I_{Sr}) and $\varepsilon Nd(T)$ values, are listed in Data Repository Table 4.

In situ zircon Hf isotopic analysis was carried out on a Neptune multi-collector ICPMS equipped with a Geolas-193 laser-ablation system (LAM-MC-ICPMS) at the Institute of Geology and Geophysics, Chinese Academy of Sciences (Beijing). Hf isotopic analyses reported in this study were obtained on the igneous zircon grains dated at ~160 Ma by SHRIMP, with ablation pit of 63 µm in diameter, ablation time of 26 s, repetition rate of 10 Hz, and laser beam energy density of 10 J/cm^2. The detailed analytical procedures were given by Xu et al. (2004). Independent mass bias factors for Hf and Yb in the isobaric interference correction were used to result in more reliable Hf isotopic data (Iizuka and Hirata, 2005). Measured $^{176}Hf/^{177}Hf$ ratios were normalized to $^{179}Hf/^{177}Hf$ = 0.7325. Zircon standards 91500 and TEMORA were analyzed alternately with the unknowns. During the course of this study, we obtained $^{176}Hf/^{177}Hf$ ratios of 0.282303±0.000008 (n=87) and 0.282677± 0.000009 (n=41) for the 91500 and TEMORA, respectively. Further external adjustment is not applied for the unknowns because our determined $^{176}Hf/^{177}Hf$ ratios for zircon standards 91500 and TEMORA are in good agreement with the reported values (Woodhead et al., 2004; Iizuka and Hirata, 2005). Hf isotopic data for zircons from the five dated granite samples are listed in Data Repository Table 5.

4. SHRIMP U–Pb geochronology

4.1. Sample MR42 (syenogranite from the northwestern Fogang Pluton)

Zircons are mostly euhedral, up to 100–150 µm long, and having length to width ratios of between 2:1 and 3:1. Most are relatively transparent and colorless, although a few are dark brown and turbid due to high uranium content. Euhedral concentric zoning is common in most crystals; no inherited zircon cores were observed. Twenty analyses of 20 zircons were obtained in sets of five scans during a single analytical session (Data Repository Table 1). They have highly variable abundance of Th (113–1304 ppm) and U (233–7112 ppm). Th/U ratios vary between 0.16 and 0.73, mostly clustering around 0.4–0.6. Common Pb is low; the proportion of common ^{206}Pb in total measured ^{206}Pb (f_{206} in Data Repository Table 1) is <1.7%. The measured $^{206}Pb/^{238}U$ ratios are in good agreement within analytical errors, and the mean yields an age of 159±2 Ma (95% confidence interval) (Fig. 2a), which is the best estimate of the crystallization age for sample MR42.
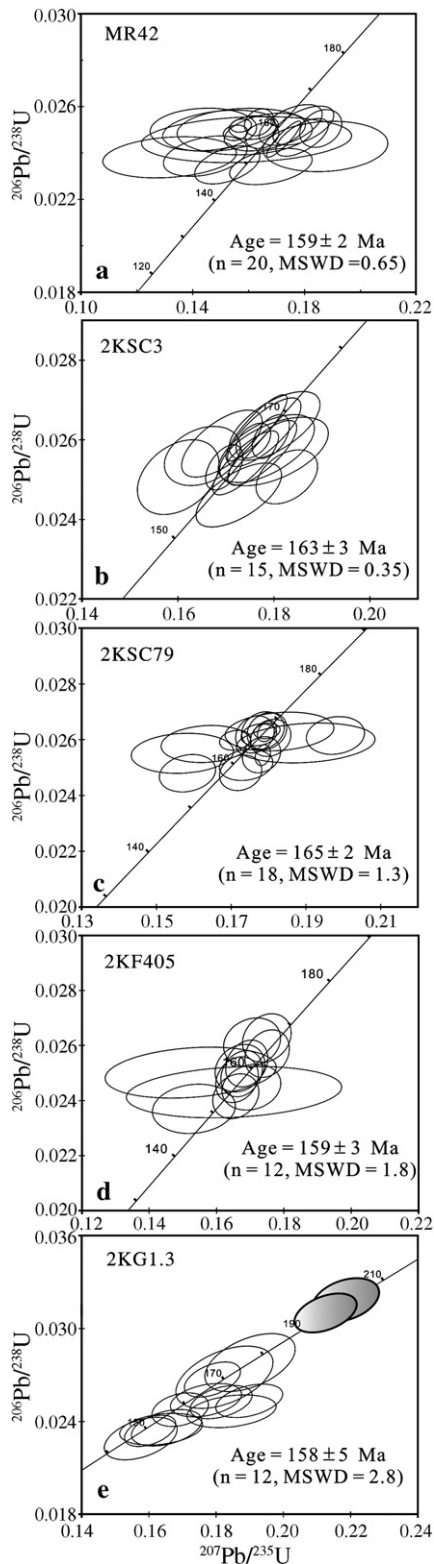
Fig. 2. U–Pb concordia diagram showing analytical data for zircons from samples (a) MR42, (b) 2KSC3, (c) 2KSC79, and (d) 2KF405 of the Fogang Batholith, and (e) 2KG1.3 of the Nankunshan Pluton.

4.2. Sample 2KSC3 (syenogranite from the southwestern Fogang Pluton)

Zircons are euhedral, up to 200 μm long, and having length to width ratios of about 2:1. Most are relatively transparent and colorless, whereas a few high-uranium crystals are dark and opaque. Euhedral concentric zoning is common in most crystals; no inherited zircon cores were observed. Sixteen analyses of 16 zircons from this sample were obtained (Data Repository Table 1). Uranium and thorium concentrations are variably high, with Th=247–1383 ppm and U=499–3003 ppm, except for spot 7.1 that has exceptionally high concentration of U (18440 ppm) and Th (5705 ppm). Th/U ratios mostly vary between 0.4 and 0.7. Common Pb is very low; with f_{206} values <0.2%. For 15 of 16 analyses, $^{238}U/^{206}Pb$ ratios agree internally to within analytical precision. The best estimate of the crystallization age of sample 2KSC3, based on the mean $^{206}Pb/^{238}U$ ratio, is 163±3 Ma (95% confidence interval) (Fig. 2b). The rejected analysis of spot 7.1 yields a $^{206}Pb/^{238}U$ age of 214 Ma, and is interpreted to be a xenocryst.

4.3. Sample 2KSC79 (biotite monzogranite from the central-western Fogang Pluton)

Zircons were mostly clear and euhedral with concentric zoning, up to 250 μm in length, and having length to width ratios of about 3:1. Rounded zircon cores are occasionally observed within a few idiomorphic grains. Twenty analyses of 20 zircons were obtained (Data Repository Table 1). Common Pb is very low; f_{206} values are all <1%, and mostly <0.2%. One analysis of zircon core (spot 6.1) is discordant and shows relatively low Th (75 ppm) and U (160 ppm), yielding a $^{207}Pb/^{206}Pb$ age 2923 Ma. The other analysis (spot 8.1) has exceptionally high concentrations of U (12369 ppm) and Th (4686 ppm), yielding a $^{206}Pb/^{238}U$ age of 201 Ma, similar to the xenocryst of spot 7.1 of sample 2KSC3. The remaining 18 analyses have variably medium to high concentrations of U (327–5689 ppm) and Th (179–2049 ppm). They have indistinguishable $^{206}Pb/^{238}U$ ratios within analytical uncertainties, corresponding to a single age population with a weighted mean $^{206}Pb/^{238}U$ age of 165±2 Ma (95% confidence interval) (Fig. 2c). This age is interpreted as the best estimate of the crystallization age for sample 2KSC79.

4.4. Sample 2KF405 (syenogranite from the Xinfengjing Pluton)

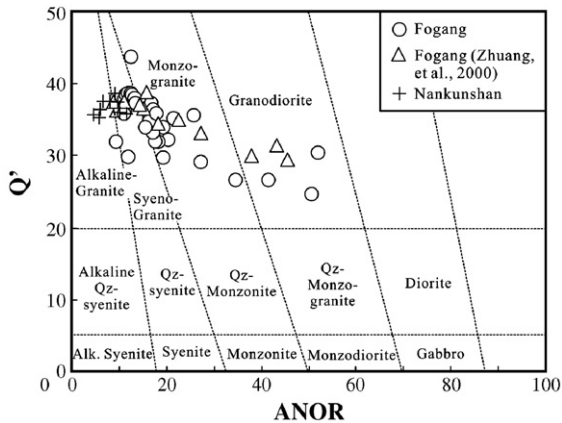Zircons are euhedral, up to 150–200 μm in length, and having length to width ratios of around 2:1 to 3:1.

Fig. 3. Q'-ANOR normative composition diagram (Streckeisen and Le Maitre, 1979) for classification of the Fogang and Nankunshan granitoids. $Q' = Q/(Q+Or+Ab+An) \times 100$; $ANOR = An/(Or+An) \times 100$.

Most are clear and colorless apart from a few dark brown and turbid crystals. Euhedral concentric zoning is common; no inherited zircon core was observed. Thirteen analyses of 13 zircons were obtained (Data Repository Table 1). They have highly variable abundance of Th (119–2374 ppm) and U (338–5038 ppm). Th/U ratios vary between 0.21 and 0.97. Common Pb is reasonably low; f_{206} values are between 0.06% and 2.3%. Spot 11.1 yields a $^{206}Pb/^{238}U$ age of 433 Ma, and is interpreted to be a xenocryst. The remaining 12 analyses have indistinguishable $^{206}Pb/^{238}U$ ratios within analytical errors, and the mean yields an age of 159±3 Ma (95% confidence interval) (Fig. 2d), which is the best estimate of the crystallization age of sample 2KF405.

4.5. Sample 2KG1.3 (alkaline granite from the Nankunshan Pluton)

Zircons are mostly euhedral, ranging between 100 and 200 μm in length, and having length to width ratios of bout 2:1. The majority of zircon grains are dark and opaque due to radioactive damages of their high-uranium contents; a few crystals are light brown in color and transparent, indicative of relatively low-uranium contents. Fourteen analyses of 14 zircons were obtained for the relatively transparent zircon grains (Data Repository Table 1). They show variably high contents of Th (955–2514 ppm) and U (1074–7175 ppm). Th/U ratios are between 0.18 and 1.04. The f_{206} values are between 0.06% and 1.0%, apart from spot 8.1 that has a f_{206} value of 2.39%. Twelve of the 14 analyses have $^{206}Pb/^{238}U$ ages ranging from 149.1±4.2 (1σ) to 176.8±7.8 (1σ). Despite a relatively large variation, these $^{206}Pb/^{238}U$ ages are indistinguishable within analytical errors. Their mean yields

a $^{206}Pb/^{238}U$ age of 158±5 Ma (Fig. 2e), which is interpreted as the crystallization age of sample 2KG1-3. Spots 4.1 and 12.1 yielded significantly higher $^{206}Pb/^{238}U$ ages of ca. 200 Ma; they are interpreted as xenocrysts.

Overall, our SHRIMP U–Pb zircon dating results, in combination with the age of 163±2 Ma for the Lapu granite (Liu et al., 2005b), indicate that the granites from the Fogang Batholith and the Nankunshan Pluton are generally synchronous and both were emplaced at ~160 Ma, despite that the Nankunshan Pluton is slightly younger as suggested by the field relationship.

5. Geochemistry and isotope results

5.1. Major and trace elements

The Fogang granites have a wide range of chemical compositions, with $SiO_2 = 63.50–77.31\%$, $Al_2O_3 = 11.68–16.10\%$, $MgO = 0.08–2.99\%$, $Fe_2O_3 = 1.35–6.37\%$, $CaO = 0.47–4.95\%$ (Data Repository Table 2). They are relatively high in total alkalis, with $K_2O = 3.08–5.92\%$ and $Na_2O = 2.35–3.87\%$, and the total $K_2O + Na_2O$ ranging from 5.43% to 9.28%. Consequently, the Fogang granites range from granodiorite to seynogranite (Fig. 3). Their A/CNK values range from 0.89 to 1.13, transitional from metaluminous to weakly peraluminous (Fig. 4), and increase with increasing SiO_2 (not shown). Al_2O_3, TiO_2, Fe_2O_3, MgO, MnO, CaO, P_2O_5, Sr and Ba decrease, but K_2O and Rb increase, with increasing SiO_2, whereas Na_2O remains nearly constant (Fig. 5). These chemical variations are consistent with the crystal fractionation of ferromagnesian minerals, plagioclase, Ti–Fe oxides and apatite.
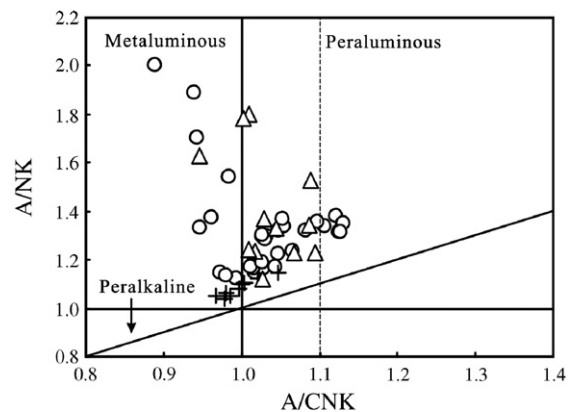

Fig. 4. A/NK vs. A/CNK plot showing the metaluminous to weak peraluminous nature of the Fogang and Nankunshan granites. $A = Al_2O_3$, $N = Na_2O$, $K = K_2O$, $C = CaO$ (all in molar proportion). Symbols are as in Fig. 3.
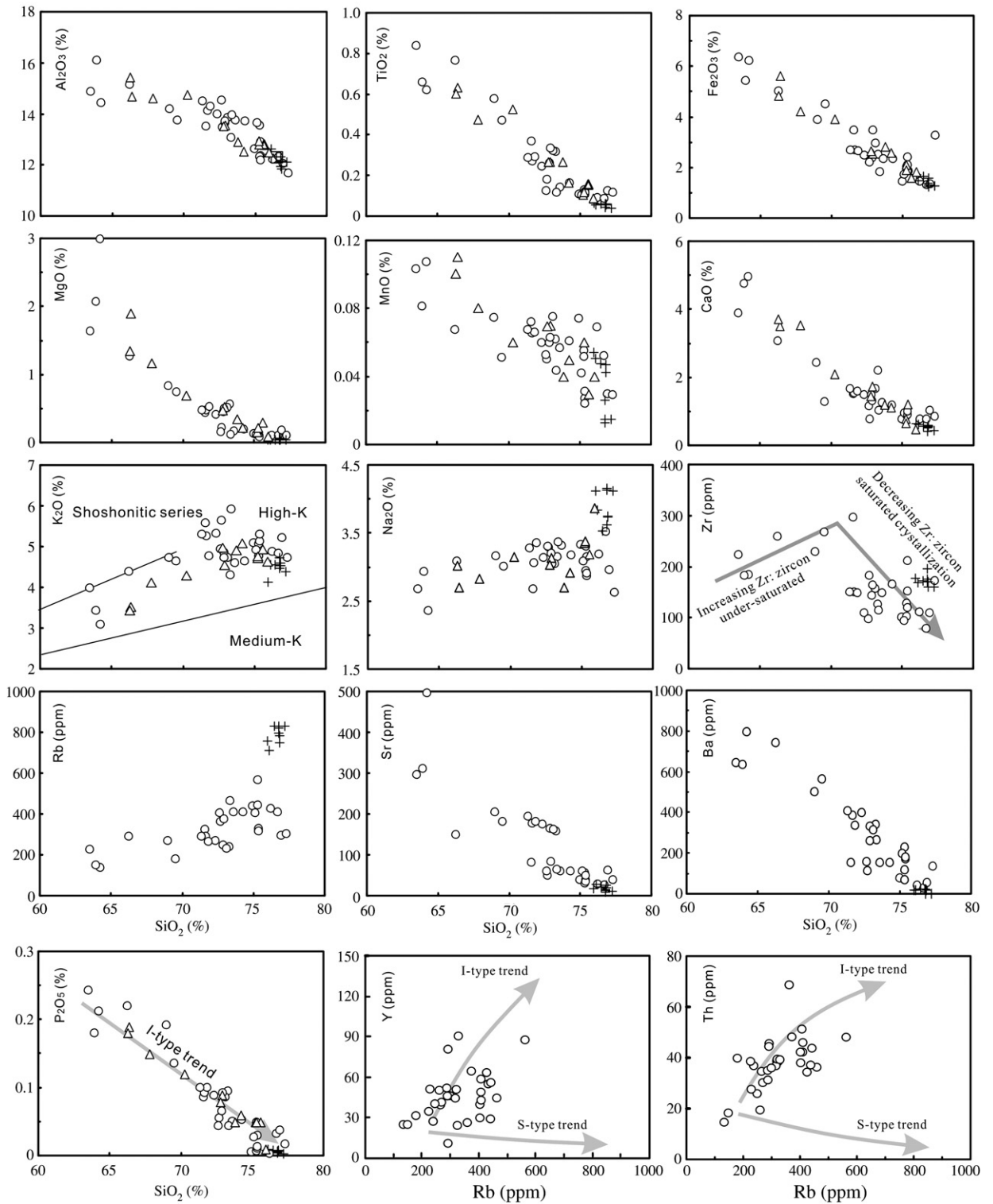
Fig. 5. Chemical variation diagrams for the Fogang and Nankunshan granites. Symbols are as in Fig. 3.

Chondrite-normalized REE patterns of the Fogang rocks invariably show light REE (LREE) enrichments and Eu negative anomalies (Fig. 6a–c). On the other hand, the REE abundances, REE pattern slopes and degrees of Eu negative anomalies change gradually with fractional crystallization (increasing SiO_2). In Fig. 6, the Fogang granites are subdivided into three groups according to their SiO_2 contents. As SiO_2 increases, LREE abundances and the REE pattern slopes decrease slightly, whereas the Eu negative anomalies increase quickly. Sample 2KSC4b

is very distinctive for its low and concave REE pattern, with an insignificant Eu anomaly due to depletion in middle REE (Fig. 6c). While such REE pattern is uncommon, it has been seen in some highly-fractionated I-type granites in NE China and was interpreted as due to separation of accessory minerals such as apatite, allanite, titanite and monazite (Wu et al., 2003). In the primitive mantle-normalized variation diagrams (Fig. 6e–g), all the Fogang rocks show enrichment in Rb and Th and characteristic depletion in Ba, Nb (Ta), Sr, P, Eu and Ti.
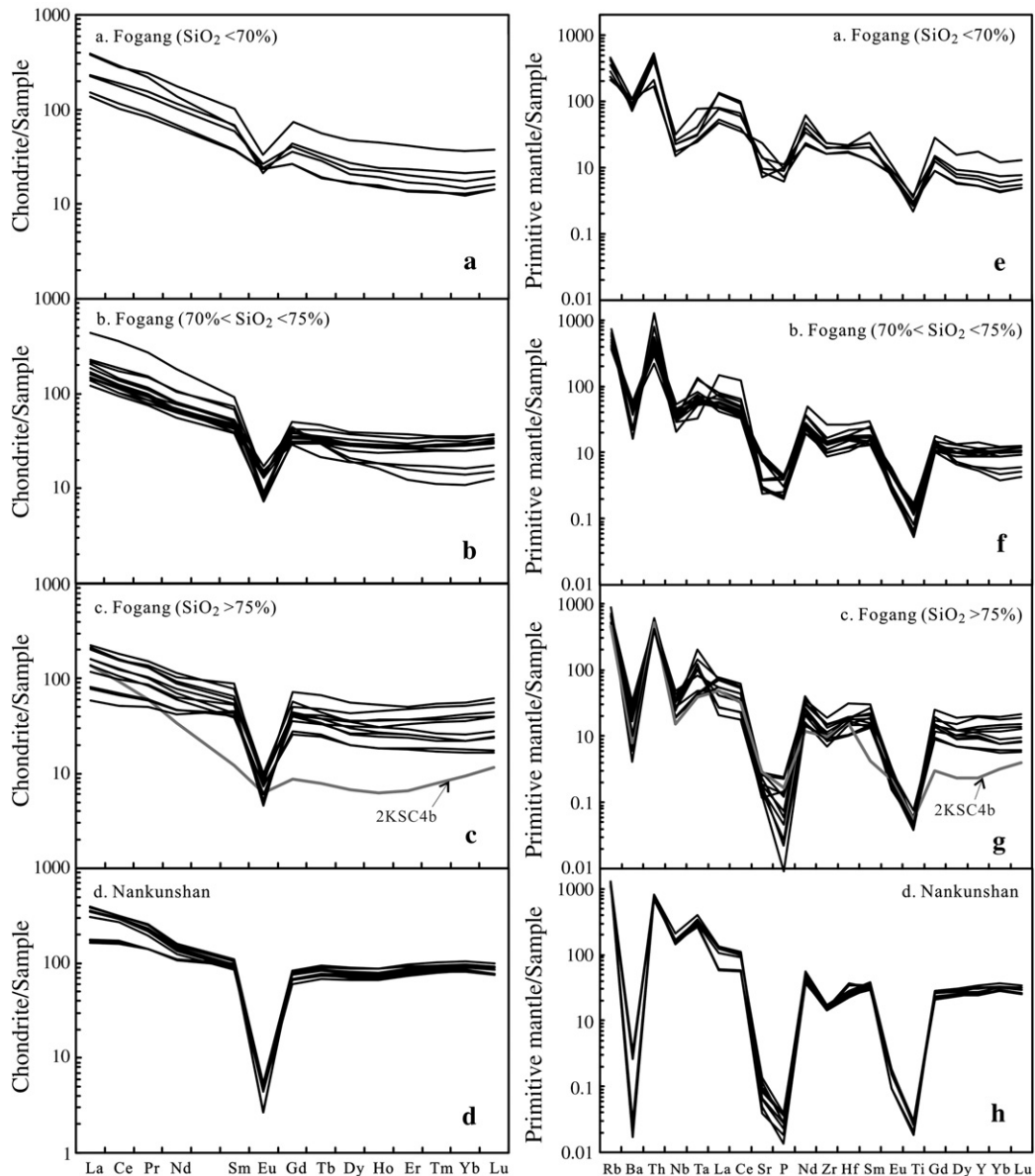

Fig. 6. Chondrite-normalized REE diagrams and primitive-mantle-normalized incompatible element spidergrams for the Fogang and Nankunshan granites. The normalization values are from Sun and McDonough (1989).
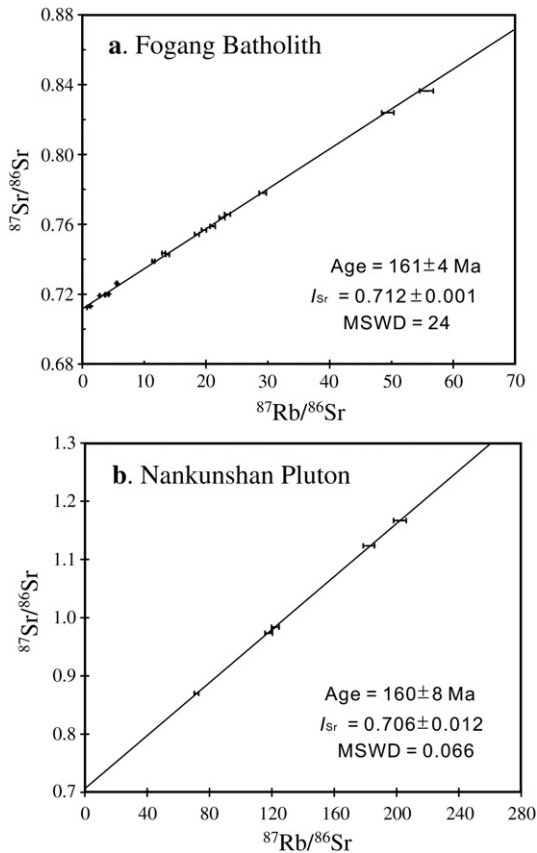
Fig. 7. Rb–Sr whole-rock isochrons of (a) the Fogang and (b) the Nankunshan granites. Age and I_{Sr} were calculated using Isoplot/Ex 2.06 after Ludwig (1999), where 0.005% and 2% were chosen as the input error of $^{87}Sr/^{86}Sr$ and $^{87}Rb/^{86}Sr$ ratios, respectively. Age errors are quoted at the 95% confidence level.

flat to moderately LREE-enriched patterns (Fig. 6d), with clear tetrad effect and pronounced Eu negative anomalies (Eu/Eu*=0.03–0.07). The $TE_{1,3}$ value that characterizes degrees of the tetrad effect (Irber, 1999) ranges from 1.08 to 1.13 (Data Repository Table 3). The spidergrams of the Nankunshan granites show some similarities to those of the high-Si granites in the Fogang Batholith, but they are strongly enriched in Th, Nb (Ta), Zr (Hf) and REE and extremely depleted in Ba, Sr, P, Eu and Ti (Fig. 6h).

5.2. Sr–Nd isotopes

Seventeen samples from the Fogang Batholith exhibit a wide range of measured $^{87}Rb/^{86}Sr$ (0.77 to 40.4) and $^{87}Sr/^{86}Sr$ (0.71247 to 0.82397) ratios due to significant fractionation and variable chemical compositions, while their age-corrected initial $^{87}Sr/^{86}Sr$ (I_{Sr}) ratios cluster between 0.7098 and 0.7136 (Data Repository Table 4). The measured $^{87}Rb/^{86}Sr$ and $^{87}Sr/^{86}Sr$ ratios form a linear-regression line, yielding an age of 161±4 Ma (Fig. 7a), identical within errors with their U–Pb zircon ages. Thus, all the analyzed Fogang samples were cogenetic. The scattering of the data, shown by MSWD=24 which is far in excess of the experimental uncertainty, is mainly attributed to the variations in initial I_{Sr} ratios. The Fogang rocks also display variable $^{147}Sm/^{144}Nd$ ratios ranging from 0.071 to 0.185, and the measured $^{143}Nd/^{144}Nd$ ratios vary between 0.51193 and 0.51239. Calculated initial $\varepsilon Nd(T)$ values range from −12.2 to −4.3 (Data Repository Table 4); the T_{2DM} model ages are mostly between 1.3 and 1.9 Ga, except for sample 2KSC3 that have a significantly older T_{2DM} model age of 2.3 Ga. There is a negative correlation between I_{Sr} and

Similarly, the degrees of enrichment in Rb and Th and depletion in Ba, Nb (Ta), Sr, P, Eu and Ti are enhanced with increasing SiO_2.

The Nankunshan granites are highly siliceous, and have a narrow range of major and trace element compositions. All samples are characterized by high contents of total alkalis, plotting in to the fields between syenogranites and alkaline granites (Fig. 3). Their A/NK values are >1, and A/CNK values between 0.97 and 1.05, falling into the areas of slightly metaluminous and weakly peraluminous in a A/CNK vs. A/NK plot (Fig. 4). Furthermore, they are characterized by extremely low abundances in Sr (8–29 ppm) and Ba (1–23 ppm), but very high in Rb (709–830 ppm) and Nb (102–148 ppm).

The Nankunshan granites are high in LREE and HREE abundance, with La_N and Yb_N being up to 390 and 105, respectively. They are characterized by nearly
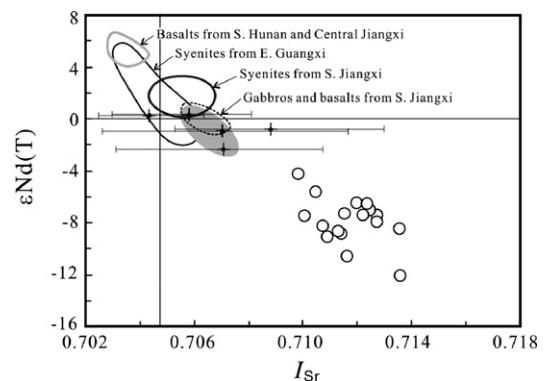

Fig. 8. Initial $\varepsilon Nd(T)$ vs. I_{Sr} diagram for the Fogang and Nankunshan granites. I_{Sr} ratios of the Nankunshan granites bear large uncertainties shown by error bars due to their extremely high Rb/Sr ratios. The grey area indicates the probable I_{Sr} range for the Nankunshan granites. Symbols are as in Fig. 3.

εNd(T) values (Fig. 8), suggesting the involvement of two major components in their origin.

Five Nankunshan samples have extremely high and variable $^{87}Rb/^{86}Sr$ (71.6 to 202) and $^{87}Sr/^{86}Sr$ (0.8699 to 1.1668) ratios. The Rb–Sr data form a tight linear-regression line corresponding to an age of 160 ± 8 Ma, comparable with their U–Pb zircon age, and an intercept $I_{Sr} = 0.706 \pm 0.012$ (Fig. 7b). The five samples have age-corrected I_{Sr} ratios ranging from 0.7044 to 0.7088 (Data Repository Table 4). It is noted that these I_{Sr} ratios bear large uncertainties (Fig. 8) due to very high Rb/Sr ratios. The Nankunshan rocks have fairly constant Nd isotopic compositions. Except for sample 2KN3.1 having relatively lower εNd(T) value of −2.4 and older T_{2DM} model age of 1.56 Ga, other four samples have a limited range of chondritic εNd(T) values (0.3 to −0.9) and T_{2DM} model ages (1.0 to 1.1 Ga) (Data Repository Table 4). In general, Sr–Nd isotopic data of the Nankunshan granites appear consistent with a binary mixing between a juvenile, mantle-derived magma and evolved crustal components for their origin.

5.3. Zircon Hf isotopes

Fifteen spot analyses were obtained for sample 2KSC3, yielding εHf(T) values between −8.6 and −10.4, corresponding to T_{DM}^C model ages between 1757 Ma and 1875 Ma. Both the εHf(T) values and T_{DM}^C model ages show nearly unimodal distributions (Fig. 9a, f), with an average of εHf(T) = −9.6 ± 0.6 and T_{DM}^C = 1820 ± 36 Ma. These Hf isotopic data indicate a major late Paleoproterozoic crustal source.

Seventeen spot analyses were obtained for sample 2KF405. Spot 9 gives the highest εHf(T) value of −5.7 and the lowest T_{DM}^C model age of 1572 Ma; spot 15 gives the lowest εHf(T) values of −11.5 and the highest T_{DM}^C model age of 1935 Ma, respectively. Results of these two analyses are significantly deviated from the remaining 15 sports with εHf(T) values = −7.0 to −10.2, corresponding to T_{DM}^C model ages = 1644 Ma to 1862 Ma. In general, all the analyses show quasi-unimodal distributions for the εHf(T) values and T_{DM}^C model ages (Fig. 9b, g), with an average of εHf(T) = −8.7 ± 1.4 and
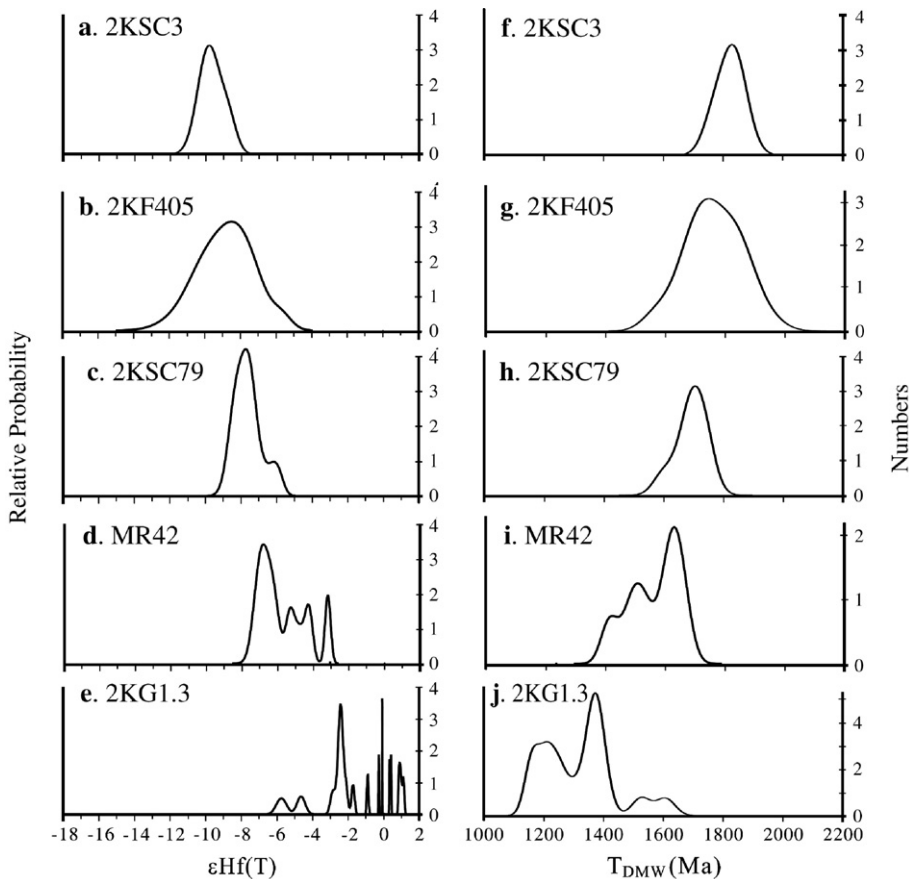

Fig. 9. Histogram of εHf(T) values and Hf model ages for the Fogang and Nankunshan granites.

$T_{DM}^C = 1764 \pm 92$ Ma. This sample has Hf isotopic compositions similar to those of sample 2KSC3, indicative of a major late Paleoproterozoic crustal source.

Sixteen spot analyses were obtained for sample 2KSC79. They show a limited range of εHf(T) values of between −5.9 and −8.4, corresponding to T_{DM}^C model ages of 1588 Ma to 1746 Ma (Fig. 9c, h). A quasi-bimodal distribution is shown for the εHf(T) values. Thirteen analyses give a mean εHf(T)=−7.9± 0.4 and T_{DM}^C model age=1710±25 Ma, and the other three analyses (spots 1, 4 and 16) yield a mean εHf(T)=−6.3±0.5 and T_{DM}^C model age=1614±28 Ma. These results suggest the involvement of a major late Paleoproterozoic crustal source with a subordinate younger component.

Fifteen spot analyses were made for sample MR42, giving εHf(T) values of −3.1 to −7.1, corresponding to T_{DM}^C model ages of 1415 Ma to 1660 Ma. These analyses display a multi-peak distribution of εHf(T) values and T_{DM}^C model ages (Fig. 9d, i). Amongst them, 8 spots form a major peak at εHf(T)=−6.6±0.4 and T_{DM}^C model age=1637±22 Ma. Other spots give higher εHf(T) values (−3.1 to −5.2) and younger T_{DM}^C model ages (1415 to 1546 Ma). A major late Paleoproterozoic crustal source and some younger components were likely involved in the origin of this sample.

Nineteen spot analyses were made for sample 2KG1.3. The determined εHf(T) values spread between 1.1 and −5.7, correspondingly, their T_{DM}^C model ages range from 1149 Ma to 1607 Ma (Fig. 9e, j). Such Hf isotopic characteristics are likely indicative of a binary mixing between a juvenile, mantle-derived magma, and an older crustal component.

Overall, Hf isotopic data for zircons from the Fogang Batholith suggests their derivation from a major late Paleoproterozoic crustal source plus variable amounts of juvenile components. The Nankunshan Granite, on the other hand, was more likely formed by mixing of a mantle-derived magma with crustal materials.

6. Discussion

6.1. Petrogenetic type: S-type, I-type or A-type?

The low-Si granites ($SiO_2 < 70\%$) of the Fogang Batholith are typical of high-K calc-alkaline I-type granites, as indicated by their metaluminous nature and the presence of hornblende. The majority of medium- to high-Si monzogranites and syenogranites, on the other hand, are highly siliceous (mostly $SiO_2 > 72\%$) and mostly hornblende-free. Chemically, they are peraluminous and high in total alkaline ($K_2O + Na_2O > 7.5\%$) and FeO*/MgO (mostly 4–15, with a few up to 24–30) due

to intensive fractionation. When dealing with highly fractionated felsic granites, there are difficulties with most petrogenetic schemes because such rocks tend to be converging major element and mineral compositions to haplogranite (King et al., 1997). This is likely the main reason that the Fogang granites were previously interpreted as S-, I- and A-types by different workers (Guangdong, 1988; Zhuang et al., 2000; Chen et al., 2002; Bao and Zhao, 2003). It is noticeable that the A/CNK values are below 1.1 for most Fogang peraluminous granites (Fig. 4), in contrast to the highly felsic S-type granites that are usually strongly peraluminous with A/CNK value much higher than 1.1 (Chappell, 1999). Furthermore, these rocks show marked decreases in P_2O_5 when SiO_2 contents are high (Fig. 5). This feature is an important criterion for distinguishing I-type granites from S-type granites because apatite reaches saturation in metaluminous and mildly peraluminous magmas (A/CNK<1.1) but highly soluble in strongly peraluminous melts (Wolf and London, 1994), and is successfully used in many studies (e.g. Chappell, 1999; Li et al., 2003b; Wu et al., 2003). The Fogang granites also show increase in Y and Th as increasing Rb, typical of I-type granite evolution trend (Fig. 5). In addition, the majority of the Fogang granites are relatively low in Zr+Nb+Y+Ce (<350 ppm) and 10,000×Ga/Al (<2.7), but high in FeO*/MgO and (K_2O+Na_2O)/CaO, falling into the fractionated granite field (Fig. 10). Thus, the
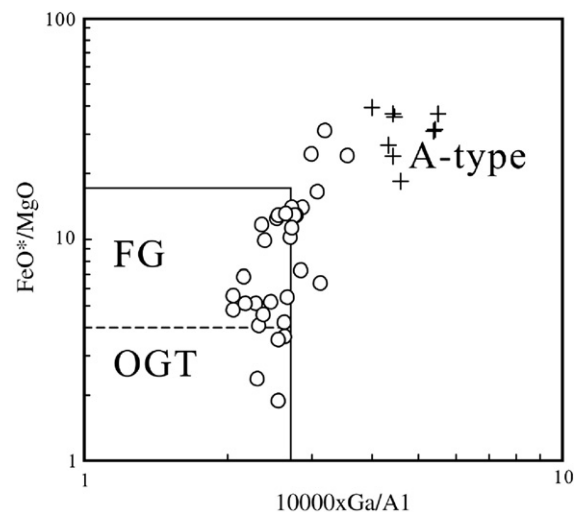

Fig. 10. FeO*/MgO vs. 10000 Ga/Al classification diagrams of Whalen et al. (1987). The Nankunshan granites are typical of A-type, whereas most of the Fogang samples falling into the highly fractionated field. FG=Fractionated M-, I- and S-type felsic granites; OGT=unfractionated M-, I- and S-type granites. Symbols are as in Fig. 3.

Fogang granites are fractionated I-type, rather than A- or fractionated S-types (Whalen et al., 1987).

The Nankunshan granites are extremely evolved in composition, thus their major element compositions are difficult to distinguish from those of the highly fractionated I-type granites in the Fogang Batholith. However, trace element compositions of the two suites are clearly distinct from each other. The Nankunshan granites are extremely enriched in HSFE and REE, showing the tetrad effect in REE patterns and some non-CHARAC trace element ratios such as Nb/Ta=8–10, Zr/Hf=15–23, K/Rb=44–53, K/Ba=1636–31710 and La/Nb=0.35–0.84. Their $10,000 \times Ga/Al$ ratios range from 4.0 to 5.5, typical of A-type granites (Fig. 10) (Collins et al., 1982; Whalen et al., 1987). Taking into account of their metaluminous to weakly peraluminous nature, the Nankunshan granites belong to aluminous A-type (King et al., 1997). Furthermore, they are very high in Nb–Ta, and low in Yb/Ta (0.93–1.53) and Y/Nb (0.84–1.49) ratios, thus can be further classified as A_1-type granites (Fig. 11a) according to the geochemical subdivision of A-type granites by Eby (1992).

6.2. Petrogenesis

6.2.1. Fogang Batholith

Geochemical characteristics indicate that the Fogang I-type granites were mainly derived from infracrustal igneous sources. Negative correlations between Sr and Nd isotopic ratios suggest that source materials consist mainly of two end-members: one having major Late Paleoproterozoic Nd model ages of ca. 1.8–1.9 Ga, $I_{Sr} \approx 0.714$, and $\varepsilon Nd(T) \approx -12$, and another relatively younger component. This interpretation is reinforced by Hf isotopic data for zircons. LAM-MC-ICPMS micro-analyses yielded large variations in $^{176}Hf/^{177}Hf$, corresponding to 2 to 6 εHf units between zircons of different growth stages within a single rock, and up to 9 εHf units between zircons within the whole suite. εHf (T) values for the analyzed zircons are generally proportional to their whole-rock $\varepsilon Nd(T)$ values. Zircons from sample MR42 have the highest $\varepsilon Hf(T)$ values between −3.1 and −7.1 that are scattered with no statistically-meaningful mean value, suggesting crystal-lization through continues hybridization of two (or more?) magmas from different sources. This sample also records the lowest I_{Sr} (0.7098) and the highest εNd (T) value (−4.3) among the analyzed granites. Thus, the $\varepsilon Nd(T)$ value of −4.3 and $\varepsilon Hf(T)$ value of −3.1 may approximate the minimum estimates, and its I_{Sr} value of 0.7098 gives the maximum estimate, for the younger or juvenile component.
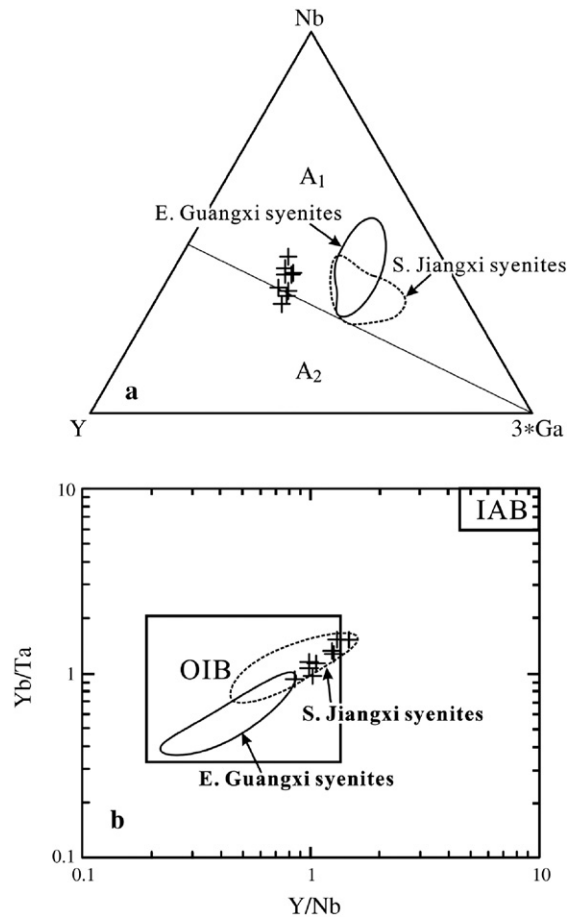

Fig. 11. Plots of the Nankunshan granites in (a) Nb–Y–Ga diagram of Eby (1992) for subdivision of A_1- and A_2-type granites, and (b) Yb/Ta vs. Y/Nb diagram of Eby (1992) exhibiting the Nankunshan rocks mostly falling into the OIB field. Syenites from southern Jiangxi (Li et al., 2003a) and eastern Guangxi (Li et al., 2004a) are plotted for comparison. Symbols are as in Fig. 3.

Calc-alkaline, I-type granitoids of intermediate-to-felsic chemistry are usually generated either by partial melting of mafic to intermediate igneous sources, or by advanced assimilation fractional crystallization of mantle-derived basaltic parental magmas. The latter process is not favored for the Fogang granites, because (1) the Fogang granites are predominantly felsic, and intermediate rocks are much less in volume, (2) Sr–Nd–Hf isotopic compositions suggest a major late Paleo-proterozoic infracrustal source for the granites, and (3) if the newly mantle-derived components played an impor-tant role in the granite origin, an older, late Archean crust component was required in view of predominant Paleoproterozoic Nd and Hf model ages. However, such late Archean rocks are lacking, or unidentified in SE China. On the other hand, the isotopic data demonstrates

that the newly mantle-derived components, despite small in proportion, might have been involved in the granite generation, consistent with the presence of mafic microgranular enclaves in the granodiorite and monzo-granite (Xu et al., 2002). We considered that the new mantle input, in addition to a mass source, likely played a more important role as heat source for the formation of the Fogang granites.

Experimental studies indicate that dehydration melt-ing of tholeiitic amphibolites may produce melts of intermediate to silicic compositions, leaving behind a granulite residue at 8–12 kbar and garnet granulite to eclogite residues at 12–32 kbar (e.g. Rushmer, 1991; Rapp and Watson, 1995). These resultant melts are usually low in K_2O and high in $Na_2O/K_2O>1$. High-pressure melting can be precluded for the Fogang granites because their HREE are not depleted, arguing against garnet as a residual mineral. All the Fogang granites are high in K_2O, having $Na_2O/K_2O<1$. Thus, tholeiitic amphibolite sources are unlikely. Using medium-to-high K basaltic compositions as starting materials, Sisson et al. (2005) obtained K-rich melts that have $Na_2O/K_2O<1$ at $SiO_2>65\%$. We thus suggest that the Fogang granitic magmas were likely generated by partial melting of infracrustal medium-to-high K basaltic protoliths heated by, and mixed to some degrees with, the contemporaneous underplating and/or intrusion of hot, mantle-derived basaltic magmas. Late Paleoproterozoic is an important timing of crustal growth in South China, and ~1.77 Ga tholeiitic and alkaline amphibolites were identified from the Cathaysia basement in NW Fujian and SW Zhejiang (Li, 1997b).

Pronounced depletions in Ba, Sr, Nb, Ta, P, Ti and Eu (Fig. 6) demonstrate an advanced fractional crystalliza-tion during the formation of these granites. Separation of Ti-bearing phases (such as ilmenite and titanite) and apatite resulted in depletion in Nb–Ta–Ti and P, respectively. Strong Eu depletion requires extensive fractionation of plagioclase and/or K-feldspar. It can be seen on Sr vs. Ba and Rb plots (Fig. 12) that Sr decreases quickly from ca. 500 ppm to ca. 150 ppm, whereas Ba changes little, varying between ca. 800 ppm and 600 ppm at the early stage of magmatic evolution, indicating separation of plagioclase. Afterwards, both Sr and Ba decrease sharply down to ca. 25 ppm and ca. 30 ppm, respectively. This is interpreted as separation of biotite and plagioclase at the late stage, rather than K-feldspar, because K_2O increases with increasing SiO, and K-feldspar megacrysts are abundant in the high-Si samples. Separation of biotite ± hornblende may explain the decreasing MgO and Fe_2O_3 during the magmatic evolution. Overall, geochemical variation is consistent
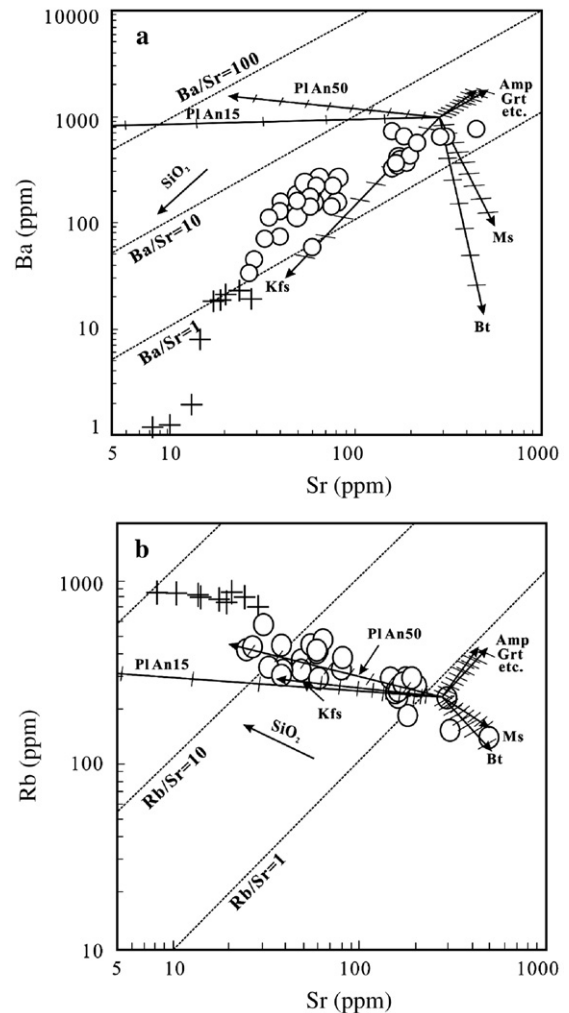

Fig. 12. (a) Sr vs. Ba, and (b) Sr vs. Rb plots for the Fogang and Nankunshan granites. Labeled vectors correspond to up to 50% fractionation crystallization of the main rock-forming minerals (after Janoušek et al., 2004). Symbols are as in Fig. 3.

with fractional crystallization of the Fogang Batholith from granodiorite, through monzogranite, to syenogra-nite, a spectrum of fractionated I-type granite suite.

6.2.2. Nankunshan Pluton

Origin and petrogenesis of A-type granites are quite controversial. Mechanisms involving melting of crustal and mantle sources, or fractional crystallization of ba-saltic magmas plus assimilation of crustal rocks, are often suggested (e.g. Collins et al., 1982; Whalen et al., 1987; Sylvester, 1989; Eby, 1992; King et al., 1997; Barbarin, 1999; Wu et al., 2002). The Nankunshan granites are compositionally similar to the aluminous A-type granites from the Lachlan Fold Belt, the latter were interpreted as being generated by high-temperature

partial melting of a felsic infracrustal source (King et al., 1997). However, this model might not be fully applicable to the Nankunshan granites. As discussed in earlier sections, Sr–Nd–Hf isotopic data suggests a binary mixing between the mantle-derived magmas and crustal melts for the origin of the Nankunshan granites. Two mechanisms may account for the involvement of these two components: (1) assimilation fractional crystallization of basaltic magmas, and (2) partial melting of felsic infracrusal sources associated with influx of mafic magmas. Aluminous A-type granites from the Lachlan Fold Belt are characterized by commonly high Y/Nb ratios, averaging at 3.2 (King et al., 1997) comparable with the Y/Nb ratio of ~3 for the lower and middle crust (Rudnick and Fountain, 1995). Thus, they are grouped into the A$_2$-type (Eby, 1992). In contrast, the Nankunshan granites are characteristically high in Nb and low in Y/Nb ratios (0.8–1.5), falling into the OIB field (Fig. 11b). In fact, geochemical and isotopic variations of the Nankunshan granites are comparable with those of the Middle Jurassic basalts, gabbros and syenites from adjacent regions of the Nanling Range (Li et al., 2003a, 2004a; Wang et al., 2005a,b,c). Thus, we prefer the first mechsanism for the origin of the Nankunshan granites, i.e. they might have been formed through extensive fractional crystallization of an asthenosphere mantle-derived alkaline parental magma assimilated with crustal components, although the second mechanism can not be totally ruled out. Those 160–165 Ma syenites from adjacent regions (eastern Guangxi and southern Jiangxi) might have shared the similar parental magmas, representing products of less fractional crystallization.

6.3. Tectonic implications

6.3.1. Major igneous event at ~160 Ma

Recent SHRIMP U–Pb zircon ages, along with reliable TIMS U–Pb zircon, Rb–Sr and Ar/Ar ages, are summarized for the Jurassic igneous rocks as a histogram (Fig. 13a). Criteria for assessing the quality of Rb–Sr and Ar/Ar ages include: (1) original data and analytical techniques were reported in the literature, or accessible; (2) Rb–Sr isochrons have good linear correlation and reasonable Rb/Sr variations and initial I_{Sr}; (3) high precision Ar/Ar ages were obtained from well-established laboratories. Fig. 13a clearly shows that the Jurassic igneous rocks, at least those precisely-dated rocks, are dominantly of 180–150 Ma in age, with a major igneous event peaked at ~160 Ma, and a subordinate phase at ~175 Ma. The early phase of igneous rocks consists mainly of bimodal intraplate mafic and A-type felsic rocks. Despite volumetrically minor, they
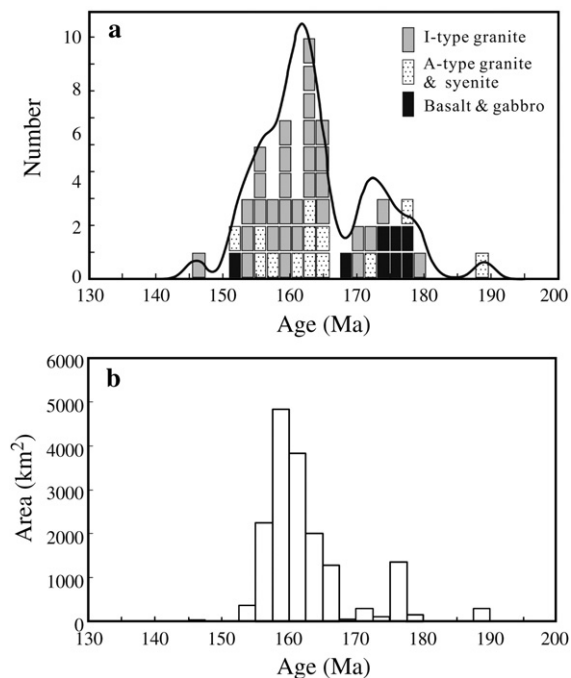

Fig. 13. Histograms of (a) ages and (b) exposed areas for the Jurassic igneous rocks. Data sources: Maruejol et al., 1990; Li, 1991; Davis et al., 1997; Zhao et al., 1998; Chen et al., 1999; Fan and Chen, 2000; Li et al., 2000, 2001; Wang et al., 2002; Li et al., 2003a, 2004a,b; Wang et al., 2004; Fu et al., 2004a,b,c; Yao et al., 2005; Yu et al., 2005; Zhou et al., 2005; Zhu et al., 2005; Liu et al., 2005a; Xu et al., 2005; Wang et al., 2006; Li and Li, 2007 and this study.

occurred sporadically within the whole hinterland. As typical rifting- and extension-related igneous associations, these mafic and bimodal rocks postdated the SE China Indosinian Orogeny (ca. 270–190 Ma, Li and Li, 2007), and signified an important onset of widespread intraplate anorogenic magmatism. A major igneous event took place between 165 and 150 Ma, constituting more than 80% of the total (dated) Jurassic igneous rocks (Fig. 13b). Among the igneous rocks formed during this time interval, weakly-peraluminous biotite monzogranites are predominant, distributed throughout the SE China hinterland. Minor amount of syenites and alkaline granites are associated closely in time and space with the biotite monzogranites. There appears to be a short igneous quiescence at ca. 150–140 Ma based on the compilation of reliable ages.

6.3.2. Intraplate magmatism rather than a broad magmatic arc?

A notable feature of the Mesozoic geology in SE China is the intensive Yanshanian magmatism, over an area of ca. 2000 km long and 1200 km width, after the

Indosinian Orogeny. While there is a general consensus that the Cretaceous (late Yanshanian) magmatism along the coastal areas occurred in an active continental margin due to the subduction of the Paleo-Pacific (Izanagi?) oceanic plate, the tectonic regime accounting for the inland Jurassic (early Yanshanian) magmatism is enigmatic and controversial. The low-angle subduction model of Zhou and Li (2000) explains the exceptionally-wide distribution of Jurassic magmatism, but is inconsistent with the development of an dominantly extensional basin-and-ranges province (Gilder et al., 1991) and the contemporaneous intraplate, rifting-related igneous rocks (Chen et al., 1999; Li et al., 2003a, 2004a; Wang et al., 2004, 2005c; Xie et al., 2005; Zhou et al., 2005). Arc-related igneous rocks derived from the mantle wedge above a subducted slab were lacking during this time, and all the Jurassic inland basaltic suites were likely originated from depleted asthenosphere mantle source.

It is generally believed that A-type granites are mostly emplaced in extensional tectonic settings (e.g. Whalen et al., 1987; Sylvester, 1989; Eby, 1992; Wu et al., 2002). The A_2-type granites represent magmas derived from continental crust or underplated crust that has been through a cycle of continent–continent collision or island–arc magmatism, whereas the A_1-type granites represent differentiates of magmas derived from OIB-like sources but emplaced in continental rifts or during intraplate magmatism (Eby, 1992). The Nankun-shan granites show geochemical affinities to the A_1-type granites (Fig. 11a). On the Nb–Y plot (Fig. 14), they plot exclusively into the within-plate field, notwith-standing their "intraplate signatures" might be enhanced by the late-stage melt–fluid interaction. Similarly, the ~160 Ma syenites (Li et al., 2003a, 2004a) are all geochemically affinitive to A_1-type granites (Fig. 11a), suggesting that they were emplaced in a common intra-plate environment. It is noteworthy that many ~160 Ma fractionated I-type biotite granites, such as those from the Fogang (this study), Hong Kong (Sewell and Campbell, 1997), Wuping (Yu et al., 2005) and Qitianling (Deng et al., 2005) are also relatively high in Nb and Y, with the majority of them falling in the within-plate granite field (Fig. 14). Such geochemical characteristics strongly argue for their emplacement in an intraplate, rather than arc, environment, consistent with their close association in time and space with the A-type granites and syenites.

6.3.3. Crustal melting by mantle upwelling during lithosphere foundering

More recently, Li and Li (2007) used a flat-slab subduction/slab-foundering model to explain the ca. 1300-km-wide Indosinian Orogen and magmatic belt in southeastern Chian, which we adopt here to explain the petrogenesis of the early Yashanian magmatism. The Indosinian Orogeny along the southeastern coast started at ~270 Ma as the (Izanagi?) oceanic plate started to subduct (Li et al., 2006). By the earliest Triassic (~250 Ma), an oceanic plateau of ~1000 km in diameter arrived at the continental arc, starting a flat-slab subduction that resulted in a craton-ward migration of the orogen over 1300 km inland to the Sichuan–Hunan border. The model suggests that by the Early Jurassic (~190 Ma), the orogenic migration ceased and the flat-slab started to break up, as indicated by the first appearance of the Keshubei A-type granite at mid-width of the waning orogen in southern Jiangxi (Fig. 15a). This important transformation from an intracontinental orogen to lithosphere extension was probably attributed to the increased gravitational pull of the flat-slab as metamorphic phase changes made it denser. Break-up of the flab-slab was further enhanced during the 180–170 Ma, causing generation of small amount of basalts and bimodal igneous rocks that were distributed sporadically in SE China hinterland (Fig. 15b). Foundering of the flab-slab likely occurred during the middle Jurassic (Fig. 15c), resulting in a strong upwel-ling of asthenosphere mantle and mafic intra- and/or under-plating. In response to a significant increase on geotherm, a major igneous event took place throughout
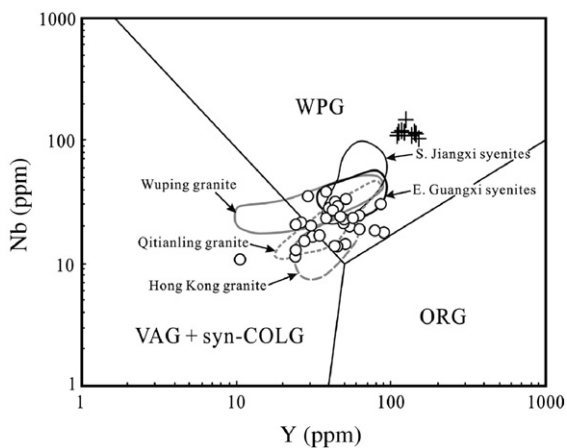

Fig. 14. Nb vs. Y diagram of Pearce et al. (1984) showing that the various types of ~160 Ma granites in SE China plotting mostly in the field of within-plate granites (WPG), including alkaline granites from Nankunshan (this study), syenites from eastern Guangxi and southern Jiangxi (Li et al., 2003a, 2004a), biotite monzogranites from Fogang (this study), Hong Kong (Sewell and Campbell, 1997), Wuping (Yu et al., 2005) and Qitianling (Deng et al., 2005). Symbols are as in Fig. 3.
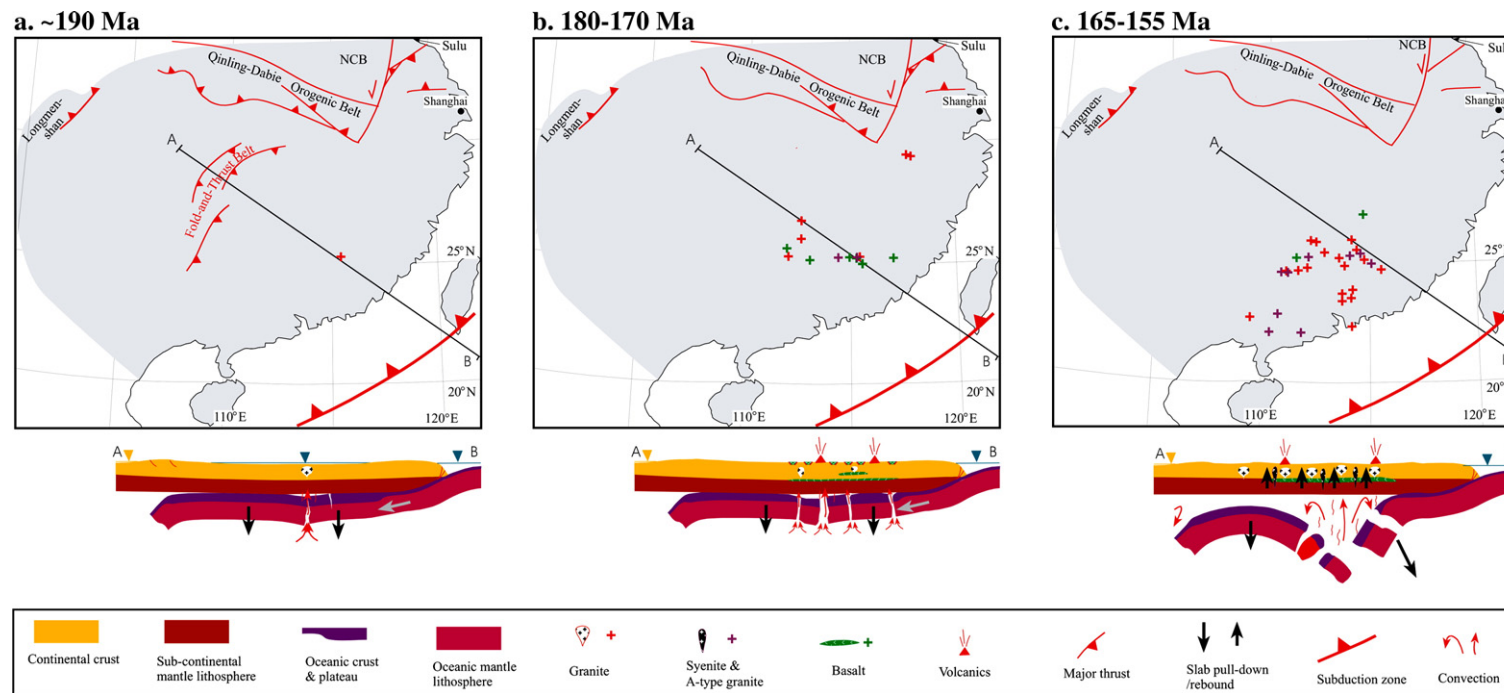
Fig. 15. Cartoon showing the tectonomagmtic evolution of SE China during the Jurassic time due to the break-up and foundering of an early Mesozoic subducted flat-slab (modified after Li and Li, 2007).

SE China hinterland, forming the widespread I- and A-type granites at ~ 160 Ma.

7. Conclusions

We draw the following conclusions based on our new results:

(1) SHRIMP U–Pb zircon dating results indicate that the Fogang and the Nankunshan granites were formed contemporaneously at ~ 160 Ma.
(2) The Fogang granites are I- and fractionated I-types, whereas the Nankunshan granites are aluminous A-type. Geochemical and Sr–Nd–Hf isotopic data suggest that the Fogang granites were derived from the Paleoproterozoic mafic-intermediate igneous protolith with small amount of addition of mantle-derived magmas. The Nankunshan rocks were likely generated through extensive fractional crystallization of asthenosphere mantle-derived alkaline parental magma associated with crustal assimilation. They are slightly younger than the 180–170 Ma intraplate basalts and/or bimodal igneous rocks, but coeval with the 165–160 Ma A-type granites and syenites in the adjacent regions.
(3) Following a subordinate phase of rifting-related magmatism at 180–170 Ma, a major igneous event took place between 165 and 150 Ma in South China hinterland. All these Jurassic igneous rocks are interpreted as anorogenic magmatism formed in response to the break-up and foundering of an early Mesozoic subducted flat-slab beneath SE China continent.

Appendix A. Supplementary data

Supplementary data associated with this article can be found, in the online version, at doi:10.1016/j.lithos.2006.09.018.

References

Bao, Z.W., Zhao, Z.H., 2003. Geochemistry and tectonic setting of the Fogang aluminous A-type granite, Guangdong Province, China — a preliminary study. Geol. Geochem. 31, 52–61 (in Chinese with English abstract).

Barbarin, B., 1999. A review of the relationships between granitoid types, their origins and their geodynamic environments. Lithos 46, 605–626.

Black, L.P., Kamo, S.L., Allen, C.M., Aleinikoff, J.N., Davis, D.W., Korsch, R.J., Foudoulis, C., 2003. TEMORA 1: a new zircon standard for Phanerozoic U–Pb geochronology. Chem. Geol. 200, 155–170.

Chappell, B.W., 1999. Aluminium saturation in I- and S-type granites and the characterization of fractionated haplogranites. Lithos 46, 535–551.

Charvet, J., Lapierre, H., Yu, Y., 1994. Geodynamic significance of the Mesozoic volcanism of southeastern China. J. Southeast Asian Earth Sci. 68, 387–396.

Chen, P.R., Kong, X.G., Wang, Y.X., Ni, Q.S., Zhang, B.T., Ling, H.F., 1999. Rb–Sr isotopic dating and significance of early Yanshanian bimodal volcanic-intrusive complex from southern Jiangxi Province, SE China. Geol. J. China Univ. 5, 378–382 (in Chinese with English abstract).

Chen, X., Wang, R.C., Liu, C., Hu, H., Zhang, W., Gao, J., 2002. Isotopic dating and genesis for Fogang biotite granites of Conghua Area, Guangdong Province. Geol. J. China Univ. 8, 293–307 (in Chinese with English abstract).

Collins, W.J., Beams, S.D., White, A.J.R., Chappell, B.W., 1982. Nature and origin A-type granites with particular reference to Southeastern Australia. Contrib. Mineral. Petrol. 80, 189–200.

Davis, D.W., Sewell, R.J., Campbell, S.D.G., 1997. U–Pb dating of Mesozoic igneous rocks from Hong Kong. J. Geol. Soc. (Lond.) 154, 1067–1076.

Deng, X.G., Li, X.H., Liu, Y.M., Huang, G.F., Hou, M.S., 2005. Geochemical characteristics of Qitianling granites and their implications for mineralization. Acta Petrol. Mineral. 24, 93–103 (in Chinese with English abstract).

Eby, G.N., 1992. Chemical subdivision of the A-type granitoids: petrogenetic and tectonic implications. Geology 20, 641–644.

Fan, C.F., Chen, P.R., 2000. Geochemical characteristics and tectonic implication of Pitou A-type granitic intrusive in South Jiangxi Province. Geochimica 29, 358–366 (in Chinese with English abstract).

Fu, J.M., Ma, C.Q., Xie, C.F., Zhang, Y.M., Peng, S.B., 2004a. The determination of the formation ages of the Xishan volcanic-intrusive complex in southern Hunan Province. Acta Geosci. Sin. 25, 303–308 (in Chinese with English abstract).

Fu, J.M., Ma, C.Q., Xie, C.F., Zhang, Y.M., Peng, S.B., 2004b. SHRIMP U–Pb zircon dating of the Jiuyishan composite granite in Hunan and its geological significance. Geotecton. Metallogen. 11, 370–378 (in Chinese with English abstract).

Fu, J.M., Ma, C.Q., Xie, C.F., Zhang, Y.M., Peng, S.B., 2004c. Zircon SHRIMP dating of Cailing granite on eastern margin Qitianling Batholith, Hunan, South China, and its significance. Geol. China 31, 69–100 (in Chinese with English abstract).

Gilder, S.A., Keller, G.R., Luo, M., Goodell, P.C., 1991. Timing and spatial distribution of rifting in China. Tectonophysics 197, 225–243.

Guangdong (Bureau of Geology and Mineral Resources of Guangdong Province), 1988. Regional Geology of Guangdong Province. Geol. Publ. House, Beijing. 941 pp.

Holloway, N.H., 1982. North Palawan Block, Philippines — its relation to Asian Mainland and role in evolution of South China Sea. AAPG Bull. 66, 1355–1383.

Irber, W., 1999. The lanthanide tetrad effect and its correlation with K/Rb, Eu/Eu*, Sr/Eu, Y/Ho, and Zr/Hf of evolving peraluminous granite suites. Geochim. Cosmochim. Acta 63, 489–508.

Iizuka, T., Hirata, T., 2005. Improvements of precision and accuracy in in-situ Hf isotope microanalysis of zircon using the laser ablation-MC-ICPMS technique. Chem. Geol. 220, 121–137.

Jahn, B.M., Chen, P.Y., Yen, T.P., 1976. Rb–Sr ages of granitic rocks in southeastern China and their tectonic significance. GSA Bull. 86, 763–776.

Janoušek, V., Finger, F., Roberts, M., Frýda, J., Pin, C., Dolejš, D., 2004. Deciphering the petrogenesis of deeply buried granites: whole-rock geochemical constraints on the origin of largely undepleted granulites from the Moldanubian Zone of the Bohemian Massif. Trans. R. Soc. Edinb. Earth Sci. 95, 141–159.

King, P.L., White, A.J.R., Chappell, B.W., Allen, C.M., 1997. Characterization and origin of aluminous A-type granites from the Lachlan Fold Belt, southeastern Australia. J. Petrol. 38, 371–391.

Lan, C.Y., Jahn, B.M., Mertzman, S.A., Wu, T.W., 1996. Subduction-related granitic rocks of Taiwan. J. Southeast Asian Earth Sci. 14, 11–28.

Lapierre, H., Jahn, B.M., Charvet, J., Yu, Y.W., 1997. Mesozoic magmatism in Zhejiang Province and its relation with the tectonic activities in SE China. Tectonophysics 274, 321–338.

Li, X.H., 1991. Geochronology of the Wanyangshan–Zhuguangshan granitoid batholith: Implication for the crust development. Sci. China, Ser B Chem. Life Sci. Earth Sci. 34, 620–629.

Li, X.H., 1997a. Geochemistry of the Longsheng Ophiolite from the southern margin of Yangtze Craton, SE China. Geochem. J. 31, 323–337.

Li, X.H., 1997b. Timing of the Cathaysia Block Formation: constraints from SHRIMP U–Pb zircon geochronology. Episodes 30, 188–192.

Li, X.H., 2000. Cretaceous magmatism and lithospheric extension in Southeast China. J. Asian Earth Sci. 18, 293–305.

Li, Z.X., Li, X.H., 2007. Formation of the 1300 km-wide intra-continental orogen and post-orogenic magmatic province in Mesozoic South China: a flat-slab subduction model. Geology 35, 179–182.

Li, X.H., McCulloch, M.T., 1998. Geochemical characteristics of Cretaceous mafic dikes from northern Guangdong, SE China: Age, origin and tectonic significance. In: Flower, M.F.J., Chung, S.L., Lo, C.H., Lee, T.-Y. (Eds.), Mantle Dynamics and Plate Interaction in East Asia, vol. 27. AGU Geodynamics, Washington, DC, pp. 405–419.

Li, X.H., Zhou, H., Liu, Y., Lee, C.Y., Chen, C.H., Yu, J., Gui, X., 2000. Mesozoic shosonitic intrusives in the Yangchun Basin, western Guangdong, and their tectonic significance. Geochimica 29, 513–520 (in Chinese with English abstract).

Li, X.H., Liang, X.R., Sun, M., Guan, H., Malpas, J.G., 2001. Precise $^{206}Pb/^{238}U$ age determination on zircons by laser ablation microprobe-inductively coupled plasma-mass spectrometry using continuous linear ablation. Chem. Geol. 175, 209–219.

Li, X.H., Chen, Z.G., Liu, D.Y., Li, W.X., 2003a. Jurassic gabbro–granite–syenite suites from southern Jiangxi Province, SE China: Age, origin and tectonic significance. Int. Geol. Rev. 45, 898–921.

Li, X.H., Li, Z.X., Ge, W., Zhou, H., Li, W., Liu, Y., Wingate, M.T.D., 2003b. Neoproterozoic granitoids in South China: crustal melting above a mantle plume at ca. 825 Ma? Precambrian Res. 122, 45–83.

Li, X.H., Chung, S.L., Zhou, H.W., Lo, C.H., Liu, Y., Chen, C.H., 2004a. Jurassic intraplate magmatism in southern Hunan-eastern Guangxi: $^{40}Ar/^{39}Ar$ dating, geochemistry, Sr–Nd isotopes and implications for tectonic evolution of SE China. In: Malpas, J., Fletcher, C.J., Aitchison, J.C., Ali, J. (Eds.), Aspects of the Tectonic Evolution of China. Geol. Soc. Spec. Publ., vol. 226, pp. 193–216.

Li, X.H., Liu, D.Y., Sun, M., Li, W.X., Liang, X.R., Liu, Y., 2004b. Precise Sm–Nd and U–Pb isotopic dating of the super-giant Shizhuyuan polymetallic deposit and its host granite, Southeast China. Geol. Mag. 141, 225–231.

Li, X.H., Li, Z.X., Li, W.X., Wang, Y.J., 2006. Initiation of the Indosinian Orogeny in South China: evidence for a Permian magmatic arc in the Hainan Island. J. Geol. 114, 341–353.

Liu, C., Chen, X., Wang, R.C., Hu, H., 2003. Origin of Nankunshan aluminous A-type granite, Longkou County, Guangdong Province. Acta Petrol. Mineral. 22, 1–10.

Liu, C., Chen, X., Wang, R.C., Zhang, W., Hu, H., 2005a. Isotopic dating and origin of complexly zoned micas for A-type Nankun-shan aluminous granite. Geol. Rev. 51, 193–200 (in Chinese with English abstract).

Liu, C., Chen, X., Wang, R.C., Zhang, A., Hu, H., 2005b. The products of partial melting of lower crust: origin of Early Yanshanian Lapu monzogranite, Guangdong Province. Geol. J. China Univ. 11, 343–357 (in Chinese with English abstract).

Ludwig, K.R., 1999. Isoplot/Ex (v. 2.06) — A Geochronological Toolkit for Microsoft Excel. Spec. Publ., vol. 1a. Berkeley Geochronology Center. 49 pp.

Martin, H., Bonin, B., Capdevila, R., Jahn, B.M., Lameyre, J., Wang, Y., 1994. The Kuiqi peralkaline granitic complex (SE China): Petrology and geochemistry. J. Petrol. 35, 983–1015.

Maruejol, P., Cuney, M., Turpin, L., 1990. Magmatic and hydro-thermal REE fractionation in the Xihuashan granites (SE China). Contrib. Mineral. Petrol. 104, 668–680.

Pearce, J.A., Harris, N.B.W., Tindle, A.G., 1984. Trace element discrimination diagrams for the tectonic interpretation of granitic rocks. J. Petrol. 25, 956–983.

Rapp, R.P., Watson, E.B., 1995. Dehydration melting of metabasalt at 8–32 kbar: implications for continental growth and crust–mantle recycling. J. Petrol. 36, 891–931.

Rudnick, R., Fountain, D.M., 1995. Nature and composition of the continental crust: a lower crustal perspective. Rev. Geophys. 33, 267–309.

Rushmer, T., 1991. Partial melting of two amphibolites: contrasting experimental results under fluid-absent conditions. Contrib. Mineral. Petrol. 107, 41–59.

Sewell, R.J., Campbell, S.D.G., 1997. Geochemistry of coeval Mesozoic plutonic and volcanic suites in Hong Kong. J. Geol. Soc. (Lond.) 154, 1053–1066.

Sisson, T.W., Ratajeski, K., Hankins, W.B., Glazner, A.F., 2005. Voluminous granitic magmas from common basaltic sources. Contrib. Mineral. Petrol. 148, 635–661.

Streckeisen, A., Le Maitre, R.W., 1979. A chemical approximation to the modal QAPF classification of the igneous rocks. Neues Jahrb. Mineral. Abh. 136, 169–206.

Sun, S.S., McDonough, W.F., 1989. Chemical and isotopic systematics of oceanic basalt: implications for mantle composition and processes. In: Saunders, A.D., Norry, M.J. (Eds.), Magmatism in the Ocean Basins. Geol. Soc. Spec. Publ., vol. 42, pp. 528–548.

Sylvester, P.J., 1989. Post-collisional alkaline granites. J. Geol. 97, 261–280.

Wang, Y.J., Fan, W.M., Guo, F., Li, H.M., Liang, X.Q., 2002. U–Pb dating of Mesozoic granodioritic intrusions in southeastern Hunan

Province and its petrogenetic implications. Sci. China, Ser. D:
Earth Sci. 45, 271–280.

Wang, Y.J., Fan, W.M., Peng, T.P., Guo, F., 2004. Early Mesozoic
OIB-type alkaline basalts in central Jiagnxi Province and its
tectonic implication. Geochimica 33, 109–117 (in Chinese with
Englsih abstract).

Wang, Q., Li, J.W., Jian, P., Zhao, Z.H., Xiong, X.L., Bao, Z.W., Xu,
J.F., Li, C.F., Ma, J.L., 2005a. Alkaline syenites in eastern
Cathaysia (South China): link to Permian–Triassic transtension.
Earth Planet. Sci. Lett. 230, 339–354.

Wang, Q., Zhao, Z.H., Jian, P., Xiong, X.L., Bao, Z.W., Dai, T.M., Xu,
J.F., Ma, J.L., 2005b. Geochronology of Cretaceous A-type
granitoids or alkaline intrusive rocks in the hinterland, South
China: constraints for late-Mesozoic tectonic evolution. Acta Pet.
Sin. 21, 795–808.

Wang, Y.J., Fan, W.M., Peng, T.P., Guo, F., 2005c. Elemental and Sr–
Nd isotopic systematics of the early Mesozoic volcanic sequence
in southern Jiangxi Province, South China: petrogenesis and
tectonic implications. Int. J. Earth Sci. 94, 53–65.

Wang, Q., Xu, J.F., Jian, P., Bao, Z.W., Zhao, Z.H., Li, C.F., Xiong,
X.L., Ma, J.L., 2006. Petrogenesis of adakitic porphyries in an
extensional tectonic setting, Dexing, South China: implications
for the genesis of porphyry copper mineralization. J. Petrol. 47,
119–141.

Wei, G.J., Liang, X.R., Li, X.H., Liu, Y., 2002. Precise measurement of
Sr isotopic compositions of liquid and solid base using (LP) MC-
ICP-MS. Geochimica 31, 295–305 (in Chinese with English
abstract).

Whalen, J.B., Currie, K.L., Chappell, B.W., 1987. A-type granites:
geochemical characteristics, discrimination and petrogenesis.
Contrib. Mineral. Petrol. 95, 407–419.

Williams, I.S., 1998. U–Th–Pb geochronology by ion microprobe. In
Applications of microanalytical techniques to understanding
mineralizing processes. Rev. Econ. Geol. 7, 1–35.

Wolf, M.B., London, D., 1994. Apatite dissolution into peraluminous
haplogranite melts: An experimental study of solubilities and
mechanisms. Geochim. Cosmochim. Acta 58, 4127–4145.

Woodhead, J., Hergt, J., Shelley, M., Eggins, S., Kemp, R., 2004.
Zircon Hf-isotope analysis with an excimer laser, depth profiling,
ablation of complex geometries, and concomitant age estimation.
Chem. Geol. 209, 121–135.

Wu, F.Y., Sun, D.Y., Li, H.M., Jahn, B.M., Wilde, S., 2002. A-type
granites in northeastern China: age and geochemical constraints on
their petrogenesis. Chem. Geol. 187, 143–173.

Wu, F.Y., Jahn, B.M., Wilder, S.A., Lo, C.H., Yui, T.F., Lin, Q., Ge,
W.C., Sun, D.Y., 2003. Highly fractionated I-type granites in NE
China (I): geochronology and petrogenesis. Lithos 66, 241–273.

Xie, X., Xu, X.S., Zou, H.B., Jiang, S.Y., Zhang, M., Qiu, J.S., 2005.
Early J₂ basalts in SE China: incipience of large-scale late
Mesozoic magmatism. Sci. China, Ser. D: Earth Sci. 35, 587–605
(in Chinese).

Xu, X.S., Zhou, X.M., Wang, D.Z., 2002. The K-feldspar megacrysts
in granites: a case study of microcline megacrysts in Fogang
granitic complex, South China. Geol. J. China Univ. 8, 121–128
(in Chinese with English abstract).

Xu, P., Wu, F.Y., Xie, L.W., Yang, Y.H., 2004. Hf isotopic
compositions of the standard zircons for U–Pb dating. Chin. Sci.
Bull. 49, 1642–1648.

Xu, X.S., O'Reilly, S.Y., Griffin, W.L., Deng, P., Pearson, N.J., 2005.
Relict Proterozoic basement in the Nanling Mountains (SE China)
and its tectonothermal overprinting. Tectonics 24. doi:10.1029/
2004TC001652.

Yao, J.M., Hua, R.M., Lin, J.F., 2005. Zircon LA-ICPMS U–Pb dating
and geochemical characteristics of Huangshaping granite in
southeast Hunan province, China. Acta Pet. Sin. 21, 688–696 (in
Chinese with English abstract).

Yu, J.H., Zhou, X.M., Zhao, L., Jiang, S.Y., Wang, L.J., Ling, H.F.,
2005. Mantle–crust interaction generating the Wuping granites:
evidence from Sr–Nd–Hf–U–Pb isotopes. Acta Pet. Sin. 21,
651–664 (in Chinese with English abstract).

Zhao, Z.H., Bao, Z.W., Zhang, B.Y., 1998. Geochemical character-
istics of the Mesozoic basalts in Hunan Province. Sci. China, Ser.
D: Earth Sci. 28, 7–14 (suppl.).

Zhou, X.M., Li, W.X., 2000. Origin of Late Mesozoic igneous rocks in
Southeastern China: implications for lithosphere subduction and
underplating of mafic magmas. Tectonophysics 326, 269–287.

Zhou, J.C., Jiang, S.Y., Wang, X.L., Yang, J.H., 2005. Re–Os isochron
age of Fankeng basalts from Fujian of SE China and its geological
significance. Geochem. J. 39, 497–502.

Zhu, J.C., Xie, C.F., Zhang, P.H., Yang, C., Gu, C.Y., 2005. Niumiao
and Tong'an intrusive bodies of NE Guangxi: petrology, zircon
SHRIMP U–Pb geochronology and geochemistry. Acta Pet. Sin.
21, 664–676.

Zhuang, W.M., Chen, S.Q., Huang, Y.Y., 2000. Geological and
geochemical characteristics of Fogang composite pluton and its
source rock. Guangdong Geol. 15, 1–12 (in Chinese with English
abstract).